Three-dimensional structure of the human copper transporter hCTR1

Christopher J. De Feo[a], Stephen G. Aller[a,1], Gnana S. Siluvai[b], Ninian J. Blackburn[b], and Vinzenz M. Unger[a,2]

[a]Department of Molecular Biophysics and Biochemistry, Yale University School of Medicine, 333 Cedar Street New Haven, CT 06510; and [b]Department of Environmental and Biomolecular Systems, OGI School of Science and Engineering, Oregon Health and Sciences University, Beaverton, OR 97006

Edited by Amy C. Rosenzweig, Northwestern Univerisity, Evanston, IL, and accepted by the Editorial Board January 22, 2009 (received for review October 13, 2008)

Copper uptake proteins (CTRs), mediate cellular acquisition of the essential metal copper in all eukaryotes. Here, we report the structure of the human CTR1 protein solved by electron crystallography to an in plane resolution of 7 Å. Reminiscent of the design of traditional ion channels, trimeric hCTR1 creates a pore that stretches across the membrane bilayer at the interface between the subunits. Assignment of the helices identifies the second transmembrane helix as the key element lining the pore, and reveals how functionally important residues on this helix could participate in Cu(I)-coordination during transport. Aligned with and sealing both ends of the pore, extracellular and intracellular domains of hCTR1 appear to provide additional metal binding sites. Consistent with the existence of distinct metal binding sites, we demonstrate that hCTR1 stably binds 2 Cu(I)-ions through 3-coordinate Cu–S bonds, and that mutations in one of these putative binding sites results in a change of coordination chemistry.

copper homeostasis | electron crystallography | EXAFS | membrane protein

Essential for life, the trace metal copper plays important roles in the reduction of superoxide anions, formation of connective tissue, metabolism of neurotransmitters and neuropeptide hormones, and the production of ATP (1). However, their redox-activity makes copper ions potentially toxic (2) and consequently, cellular availability of copper is highly regulated by an intricate network of intracellular chaperones, transcription factors and membrane transporters (3–6). Although much is known about intracellular copper chaperones, the mechanisms of copper translocation across cellular membranes are less well understood. At the protein level, 2 families of membrane proteins control cellular copper uptake and secretion: copper export is governed by the ATP-dependent pumps ATP7A and ATP7B (7, 8), whereas copper import is mediated by CTR-proteins through unknown mechanisms independent of ATP hydrolysis (9). The ATPases have been studied more because single point mutations in these proteins cause Menkes and Wilson disease (10–12). In contrast, CTR-proteins, do not seem to be causal for specific diseases but are essential nevertheless as CTR knockout is embryonic lethal in mice (13, 14).

Although important, the detailed mechanisms of copper movement across membranes remain unknown and were recently confounded by the finding that both copper transporting ATPases and CTR proteins contribute to membrane transport of the chemically unrelated antitumor drug cisplatin (15–17). Here, we describe the structure of the human copper transporter, hCTR1, at 7 Å resolution in the plane and 15 Å in the vertical direction. The structure shows how 3 subunits of a symmetric trimer form a channel-like permeation pathway for copper, and how copper movement across the membrane can be controlled. Moreover, the architecture of hCTR1 suggests that the transporter mimics the structural equivalent of transition states during copper transfer reactions between copper chaperones and their respective targets (5, 18). Taken together, these findings represent a major step forward in the mechanistic understanding of copper permeation across membranes.

Results

hCTR1 Molecules Pack Tail-To-Tail in a Double-Layered Crystal Form. We reported the projection structure of hCTR1, obtained from a double-layered crystal form with p622 plane group symmetry (19). The projection revealed that hCTR1 is trimeric and suggested that the trimer contains a pore along the central 3-fold axis. However, the shape of the putative membrane conduit for copper ions remained unknown, and no details could be derived about the arrangement of the transmembrane helices both within the monomer and the trimer. We therefore extended the analysis by recording images of crystals tilted up to ≈46° (Table 1). The final reconstruction was calculated to an in plane resolution of ≈7 Å in the plane of the membrane and ≈15 Å in the vertical direction. The 3D-data confirmed the double-layered nature of the crystal form as it showed 2 well-resolved layers of hCTR1 trimers that were related by 2-fold axes (Fig. 1*A*). ImmunoGold labeling of the crystals revealed that the transporter molecules in the 2 layers were packed tail-to-tail with the intracellular C-terminal domains facing each other, because only antibodies recognizing extracellular parts of the transporter were able to bind to the surfaces of the crystals (Fig. 1*E* and *F* and Figs. S1–S3).

hCTR1 Contains a Cone-Shaped Pore at the Center of the Trimer. When seen from the direction parallel to the membrane, each hCTR1 trimer appeared as a compact molecule with dimensions of ≈85 × 45 × 45 Å. Within the central region of the trimer, 9 well-resolved rods of density were observed that spanned a distance of at least 30 Å (Fig. 1*A*). At ≈7 Å resolution, the spacing and dimensions of these densities were consistent with those of α-helices and therefore were likely to represent the transmembrane helices (TM) of the transporter. The structure thus confirmed that each hCTR1 monomer spanned the bilayer 3 times (see Fig. S4*A* for topology diagram). A longitudinal section (Fig. 1*B*) revealed a cone-shaped internal vestibule that stretched across the entire membrane along the 3-fold axis of the trimer. At its narrow end toward the extracellular exit, the pore measured ≈8 Å across, neglecting the contribution of sidechains, and only a single TM from each monomer contributed to the lining of the pore in this region, reminiscent of the structural design of classical channel proteins such as potassium or mechanosensitive channels (21–23). Toward the in-

Author contributions: N.J.B. and V.M.U. designed research; C.J.D.F., S.G.A., and G.S.S. performed research; C.J.D.F., N.J.B., and V.M.U. analyzed data; and C.J.D.F. wrote the paper.

The authors declare no conflict of interest.

This article is a PNAS Direct Submission. A.C.R. is a guest editor invited by the Editorial Board.

Freely available online through the PNAS open access option.

Data deposition: The structure reported in this paper has been deposited at the Electron Microscopy Data Bank, www.ebi.ac.uk/msd/emdb (accession no. EMD-1593).

[1]Present address: Department of Cell Biology, The Scripps Research Institute, 10550 North Torrey Pines Road, La Jolla, CA 92037.

[2]To whom correspondence should be addressed. E-mail: vinzenz.unger@yale.edu.

This article contains supporting information online at www.pnas.org/cgi/content/full/0810286106/DCSupplemental.

Table 1. Summary of structural statistics

Parameter	Value
No of images	58
Unit cell parameters	
a, Å	89
b, Å	89
γ, °	120
Two-sided space group	p622
Range of crystal tilts, °	1.2–46.2
Range of underfocus, Å	≈4,000–15,000
Total no. of measurements	13,764
Total no. of fitted measurements	1,147
Effective resolution cutoffs*, Å	
In-plane	7
Vertical	15
% complete to 6 Å in plane with 40° tilt	79
Overall weighted phase residual†	19.0

*Measured from the point spread function of the fitted data set (20).
†For fitted lattice lines, including data to IQ8 and to a nominal in-plane resolution of 6.0 Å.

tracellular end, the pore widened into a large and presumably aqueous cavity, measuring ≈22 Å across. This change in pore diameter was caused by a pronounced rearrangement of the helix packing, which morphed from a triskelion-shaped arrangement at the extracellular side into an even distribution of the helices around the pore at the intracellular side of the membrane (Fig. 1 *C* and *D*).

Second Transmembrane Helix Is the Principal Pore Lining Helix of hCTR1. To obtain further insights into the structure and possible mechanism of copper transport, we assigned the helices in the map to the helices in the amino acid sequence. Based on the constraints given by our ImmunoGold-labeling results, biochemical data and clues in the density map itself, the assignment shown in Fig. 2 emerged as the most likely out of 12 possible models (six for each of the 2 possible orientations of the trimer with respect to the bilayer). In this assignment, TM1 was pinched between TM2 and TM3 from the same monomer, which resulted in a topology shared with the "3-helix bundle" architecture that is observed within the larger bundles of transporters in the major facilitator family (24, 25). Toward the intracellular side, contacts between subunits were mediated by interactions between TM2 and TM3 from adjacent monomers, whereas close to the extracellular side of the membrane all interactions between monomers were mediated by TM2. This design placed TM2 at the center of the trimer in the narrowest part of the pore, making TM2 the singly most important TM-segment to define the pore itself. Notably, the density map suggested that functionally important methionine residues within a MxxxM-motif at the extracellular end of TM2 (26–28) resided in close apposition to each other. To test this prediction, we generated a M154C mutant in a cysless background of hCTR1 (Fig. 2*F* and Fig. S5). As shown in Fig. 2*G*, this mutant was able to form a disulfide bond, indicating that symmetry related positions of M154 approached each other very closely within the trimer (Fig. S5*D*). In contrast, a TM2 H139C mutant did not form disulfide-linked monomers, which was consistent with the structure as observed. Interestingly, the H139C mutant also was less efficient at forming trimers than the other mutants used for this study (Fig. S5 *A* and *B*). This suggested that H139 might be involved in interactions between monomers, rather than acting as potential ligand for copper ions (26).

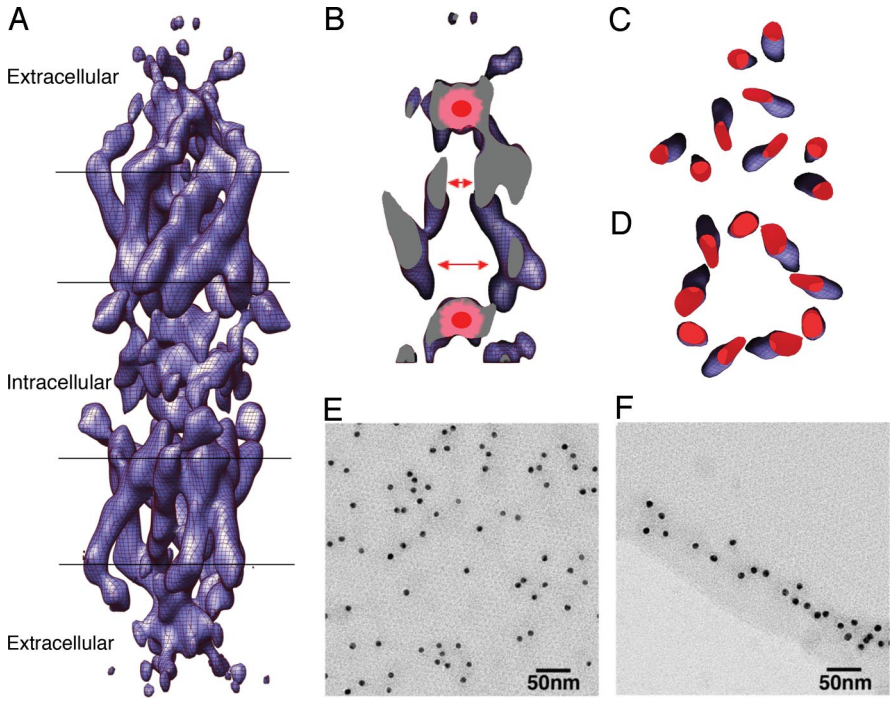

Fig. 1. Molecular organization of hCTR1. (*A*) Side view of a CTR1 dimer-of-trimers that constitutes the basic building block of the 2D-lattice (contoured at 2σ above mean). Solid black lines indicate the approximate boundaries of the hydrophobic core of the membrane, assuming a thickness of 30 Å. The orientation (topology) of the trimers in the 2 layers was derived from gold labeling of hCTR1 2D crystals (*E* and *F*) and immuno-precipitation experiments using WT and cysless hCTR1 (Fig. S3). (*B*) Slab of a longitudinal section through the middle of one trimer molecule illustrating the shape of the membrane-spanning pore. Red double-headed arrows mark the narrowest (≈8 Å, side chains neglected) and widest part (≈23 Å, side chains neglected) of the pore. Areas marked red correspond to extramembraneous densities that cap the pore at its ends. (*C* and *D*) 10 Å wide cross-sectional slabs taken from the extracellular (*C*), and intracellular (*D*) end of the membrane domain illustrate how the 9 TMs (three from each subunit) form the pore. (*E* and *F*) Representative examples of ImmunoGold labeling experiments demonstrating that the extracellular hemagglutinin epitope (HA) of the recombinant HA-hCTR1^{N15Q} is accessible on the surface of the 2D lattice (*E*) whereas an epitope contained in the intracellular C terminus of hCTR1 is accessible only along the edges of crystals (*F*).

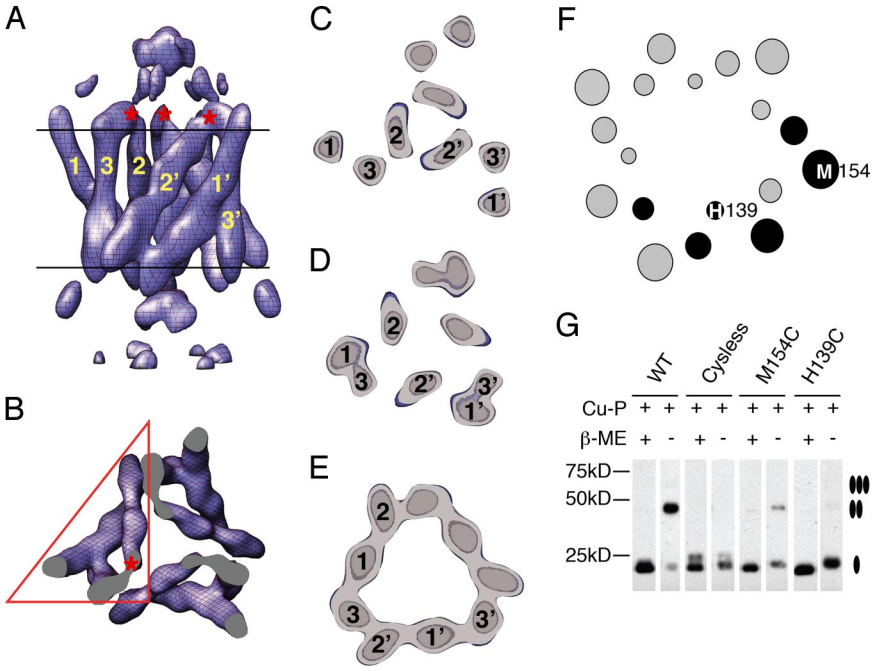

Fig. 2. Helix assignment. (*A*) Side view of a HA-hCTR1^{N15Q} trimer (contoured at 3σ above mean) reveals a direct connectivity (red asterisks) between 2 TM-segments on the extracellular side of the membrane. TM segments are labeled with the number of the corresponding TM segments in the sequence (1 = TM1, 2 = TM2, 3 = TM3). Assignments are shown for 2 subunits (TM123 and TM1′2′3′ respectively). (*B*) Top view looking down the 3-fold axis as seen from the extracellular side. The putative assignment of the subunit boundary (red triangle) and the short loop (red asterisk) connecting TM2 and 3 are shown. (*C–E*) Cross-sections through the membrane embedded domain. (*E*) Extracellular side. (*D*) Middle of the bilayer. (*E*) Intracellular side. Numbering of helices is as described for *A*. (*F*) Helical wheel plot of TM2. Nonpolar residues are colored gray. Black coloring indicates residues that are polar or possess metal binding properties. Residues His-139 and Met-154 are explicitly labeled because they were individually replaced by cysteine for disulfide cross-linking experiments. (*G*) Disulfide cross-linking of recombinant, purified HA-hCTR1^{N15Q}(WT), HA-hCTR1^{N15Q,C161A,C189A} (Cysless), HA-hCTR1^{N15Q,C161A,C189A,M154C} (M154C), and HA-hCTR1^{N15Q,C161A,C189A,H139C} (H139C). Proteins were incubated in the presence of copper phenanthroline (Cu-P) to facilitate disulfide bridge formation, separated and blotted. Ovals to the right indicate the mobility of hCTR1 oligomeric species in SDS. Similar results were obtained without use of Cu-P. Dimer formation of WT is through disulfide bridge formation between cysteines in the C-terminal HCH-sequence of 2 subunits of the hCTR1 trimer (19, 37). White separation between lanes indicates that some data were taken from separate gels.

TM3 Is Involved in Tight Helix Packing. Further evidence for the model came from the observation that TM2 showed a direct connectivity to one of the adjacent helices on the extracellular side of the membrane (labeled by red asterisks in Fig. 2 *A* and *B*). Coincidentally, the loop that connects TM2 to TM3 on the extracellular side of the membrane is predicted to consist of only 3 residues (Fig. S4). This was consistent with the density map, and identified TM3 as the helix that was the most perpendicular to the membrane plane. Notably, the presence of an abundance of small amino acids—including the structurally important GxxxG-motif (29)—allowed TM3 to approach TM1 of the same monomer so closely that the 2 helices were not completely resolved at 7 Å in plane resolution (Fig. 2*D*). Supporting the idea that the GxxxG-motif may contribute to tight helix packing between TM1 and 3, similar "merging" of helix cross-sections was observed in regions harboring GxxxG-motifs in other membrane proteins when their known crystal structures were filtered to the lower resolution of our reconstruction (Fig. S6). Having assigned both TM2 and TM3 left only one choice for TM1, thus completing the assignment of helices in the density map.

hCTR1 Stably Binds 2 Cu(I) Through 3-Coordinate Cu–S Bonds. The model that emerged from assigning the TM-helices suggested that Met residues of the MxxxM-motif on TM2 could contribute directly to copper conduction along the central pore of hCTR1 by providing a closely spaced pair of 3-coordinate binding sites for the ion. Resonating with the idea that copper moves across the plasma membrane by exchange between binding sites, additional features, capping the pore at both ends (Figs. 1*B* and 2*A*, and Fig. S7), were positioned about the 3-fold axis of the trimer. Located outside the membrane, these additional densities must have been formed by the N-terminal and intracellular domains of hCTR1, suggesting that the extramembraneous regions of CTR1 provided important structural elements that regulated copper access to and from the pore. Indeed, previous biochemical studies established the importance of an MPM-sequence motif in the N terminus of CTR-proteins (26–28) and, Cys-containing clusters of metal binding amino acids are found at the C termini of many CTR-proteins. Interestingly, the copper binding ability of these Cys-containing sequences has been implicated in playing important roles in CTR1 function (30–32) (Fig. S4). An attractive hypothesis was that the MPM-motif and HCH-sequence were located within the additional density features that guarded the ends of the copper permeable pore in the density map. This hypothesis implied that hCTR1 should contain distinct Cu(I)-binding sites. To test this idea, we determined the copper binding properties of WT hCTR1 and a cysless mutant that lacked the potential sulfur-ligand in the C-terminal HCH-sequence of the hCTR1 sequence. Inductive plasma-optical emission spectroscopy (ICPOES) indicated that each of these proteins stably bound 2 Cu(I)-ions per trimer (See Fig. 3*C*). This result could have been fully accounted for by Cu(I)-coordination through the N-terminal MPM- and TM2 MxxxM-motifs, which would also explain why mutating the C-terminal HCH-sequence to HAH in the cysless hCTR1 did not change the stoichiometry of Cu(I)-binding. However, ICPOES does not reflect the actual chemistry of metal coordination. Therefore, a contribution of the C-terminal HCH-/HAH-sequence could still have been

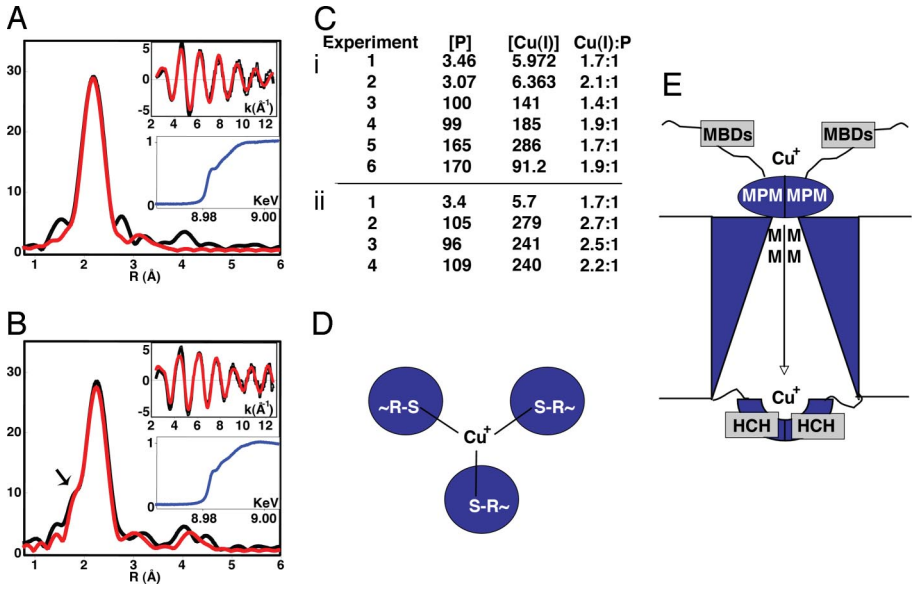

Fig. 3. Copper binding by hCTR1. (*A* and *B*) Fourier transform and EXAFS (*Upper Inset*) for WT HA-hCTR1^{N15Q} (*A*) and cysless hCTR1 (*B*). Black lines represent experimental data, simulations are shown in red. The appearance of a shoulder (arrow in *B*) indicates the involvement of Cu-N(His)coordination. Blue *Insets* are absorption edges in the region 20 keV below to 20 keV above the edge jump. The weak shoulder at 8.985 keV on the edges is typical of 3-coordination. Parameters used to simulate the data are given in Table S1. Only the best fit is shown for the cysless mutant (see Fig. S8 for comparison with fit for one 3-coordinate Cu–S(Met) site and one 3-coordinate Cu-N(His)-site). (*C*) Copper binding data obtained by independent ICP-OES experiments for WT-hCTR1 (*i*) and cysless-hCTR1 (*ii*) respectively. P, protein. Concentrations are micromolar. (*D*) Scheme illustrating how 3 subunits of the timer construct an appropriate geometry for copper coordination through symmetry related sulfur-bearing residues. (*E*) Diagram illustrating the putative trajectory of copper through the pore, and how alignment of external copper binding sites with the central pore would provide a series of checkpoints to ensure regulated copper movement through hCTR1. ''MBD''s refer to the multiple metal binding residues found in the N-terminal domain, and MPM, M, and HCH refer to the amino acid residues that are involved in the formation of defined and highly conserved putative metal binding sites as discussed in the text.

possible if in the cysless mutant Cu(I) ions were coordinated by His residues. To resolve this issue, we turned to extended X-ray absorption spectroscopy (XAS) to determine the coordination chemistry of the bound copper ions in both the WT and cysless hCTR1 transporters. For the WT protein, the data were best simulated by 3 Cu–S interactions per binding site at 2.25 Å (Fig. 3*A* and Table S1), consistent with the hypothesis that both Cu(I) ions were bound either by Cys, Met or both (e.g., MPM-motif, MxxxM-motif, HCH-motif). In contrast, the cysless protein exhibited an altered EXAFS spectrum that showed the appearance of Cu-N(His) coordination (Fig. 3*B*). The easiest explanation for this observation was that the C-terminal HCH-/HAH-motif contributed to Cu(I)-binding in both proteins because the appearance of Cu-N(His)-coordination and the lengthening of the Cu–S bond to 2.31 Å (which is more typical of Cu–S(Met) than Cu–S(Cys) (33, 34)) were a consistent with a replacement of the lost cysteine ligands by histidines (see Table S1 for details on fits of the EXAFS data). Although additional studies, will be required to fully establish the contribution of multiple binding sites to copper capture, transport and distribution, the data presented here are the first direct proof that hCTR1 can bind Cu(I) through distinct binding sites, and that the trimer is able to stably accommodate 2 copper ions.

Discussion

Recent years have seen much progress in elucidating the mechanistic details of copper trafficking within cells (18, 35). In contrast, the mechanism of copper movement across cellular membranes has been elusive, in part because no detailed structural information had been available for copper transport proteins of the CTR-family or the copper transport ATPases. Extending our previous projection structure, the 3D-structure of hCTR1 reveals that overall the transporter conforms with the design of a ''traditional'' ion channel in which a membrane spanning pore is created by symmetry related TM-segments from multiple subunits of a symmetric oligomer (19). Furthermore, the strictly conserved MxxxM-sequence motif on TM2 of CTR-proteins provides ligands that are likely to bind Cu(I) during passage, reminiscent of the selectivity filter in K-channels (22). Supporting this idea, the TM2 M154C-variant of hCTR1 can form disulfide-linked dimers, which places the symmetry related methionine residues in direct vicinity to the 3-fold axis. Moreover, the EXAFS data demonstrated 3-coordinate Cu(I)-binding, which to date is the most compelling evidence that copper moves at the interface between subunits of the CTR trimer.

Although the structure, EXAFS, and biochemical data all argue for a participation of the MxxxM-motif in Cu(I) transport, the exact mechanism of their contribution remains unknown. In the simplest case, the sulfur atoms of the 2 ''triangles'' of methionine residues form a ''static slide'' that allows copper to pass along. Alternatively, the 2 consecutive binding sites may be ''out of register'' or, even more extreme, only 1 of these 2 binding sites may adopt the proper geometry for Cu(I)-binding at any one time. Any mechanism involving these latter 2 cases implies that passage of copper is associated with conformational changes. Interestingly, 3 independent lines of biochemical evidence all point toward a mechanism that involves conformational changes during transport: (*i*) fluorescence resonance transfer studies suggest that the C termini move during copper transport in yeast CTR1 (36), (*ii*) high-extracellular copper concentrations result in a clearance of hCTR1 from the cell surface (which can only happen if the occupancy of extracellular Cu(I)-binding sites is communicated to the intracellular side of the membrane) (28) and (*iii*) trypsin digestion of hCTR1 in the absence or presence of copper ions results in different proteolytic cleavage patterns (37). In addition to these observations, our own studies are also suggestive of a mechanism that involves different conformational states. First, the EXAFS data demon-

strated that the 2 bound ions were spatially well separated because no copper clusters were detected in the spectra for either WT or cysless hCTR1. Chemically, this separation makes sense because the presence of large distances between the potential metal binding sites at the N and C termini and the sites furnished by the MxxxM-motif on TM2 may require copper release from and recapture by the protein as the ion travels through the membrane. Because this would generate solvated Cu(I), direct collision between copper ions must be avoided to prevent disproportionation to Cu (0) and Cu(II), suggesting that any movement of copper ions through CTR1 needs to be highly coordinated. Second, biochemical evidence shows that the Met residues in the MxxxM-motif can be replaced by Cys or His residues (27), and even abrogation of one of the sites through substitution by Ile residues is compatible with transport (26). This suggests that at a minimum this region of the structure is very flexible and therefore may not act as a static slide for Cu(I)-ions. Notably, the short loop connecting this region to TM3 and the fact that TM2 also packs against TM3 of the neighboring subunit (Fig. 2 *C–E*) would allow the status of the MxxxM-motif to be communicated very efficiently to other parts of the monomer and trimer, and therefore, this region seems to be a good candidate to serve as a conformational switch. We therefore favor a model in which CTR-proteins transport copper through a chain of copper exchange reactions between defined Cu(I)-binding sites, and that these exchange reactions involve well-defined conformational switches (Fig. 3 *D* and *E*). Intriguingly, the trimeric structure of CTR-protein is ideally suited for a mechanism that is based on metal exchange reactions because it mimics the 3-coordinate transition states that occur during copper exchange reactions between intracellular copper chaperones and their targets (5, 18). Kinetically controlled copper movement through CTR1 would also explain its independence from ATP-hydrolysis because the putative C-terminal binding site furnished by the HCH-sequence would provide a thermodynamic sink because of the higher stability of Cu(I)-Cys coordination compared with Cu(I)-Met. Taken together, our studies represent an important step toward the understanding of copper movement across the plasma membrane and provide a rich template for future mechanistic studies of copper transport.

Methods

Crystallization. Two-dimensional crystals were prepared essentially as described in ref. 19. Briefly, 0.5 mg of 1,2-dioleoyl-*sn*-glycero-3-phosphocholine (DOPC) (Anatrace) were dried down, washed in hexane, and then solubilized in 10 mM Mops pH 7.4, 280 mM NaCl, 2 mM EDTA, and 60 mM *n*-octyl β-D-glucopyranoside (Anatrace). Gel-filtered hCTR1 (0.8–1 mg/mL) was then added to solubilized lipids to a protein:lipid ratio of 1.5:1 (final protein 37 μg), and mixed for 1 h at 26 °C. Detergent was removed by dialysis (Pierce Slide-A-Lyzer MINI Dialysis Units) against detergent-free buffer for 21–24 h at 26 °C.

Sample Preparation. 300 mesh gold grids (Electron Microscopy Science) or acid-washed molybdenum grids (Pacific Grid-Tech) were coated with continuous carbon. Before use, grids were glow-discharged in air and vitrification was carried out manually. Gold grids were used for collecting data from specimens at low tilt angles, whereas molybdenum grids were used mostly to collect data of samples tilted to >20°.

Image Acquisition. Images were collected on a Tecnai F20 field-emission microscope, operated at 200 keV, liquid nitrogen temperatures, magnification of 50,000×, and mean underfocus ranging from 4,000 to 15,000 Å. Samples were mounted on GATAN 622 side-entry cryoholders. Images were recorded at 10–12 e/Å^2. Nominal sample tilts were in the range of 0–46°. Images were recorded on Kodak SO-163 film and developed for 12 min in full-strength Kodak D19 developer.

Film Scanning and Image Processing. Electron micrographs were digitized using a Zeiss SCAI scanner (7-μm pixel size corresponding to 1.4-Å resolution at the specimen level). Data were processed using the MRC software package (38–40), and following standard procedures (additional image processing steps included in the *SI Materials and Methods*). Volumes were calculated in CCP4 (41) using a negative *B*-factor of 300 Å^{-2}. Volumes were rendered in Chimera (supported by National Institutes of Health P41 RR-01081; www.cgl.ucsf.edu/chimera) (42) for viewing and preparation of figures. For clarity, densities from neighboring molecules on the lattice were removed manually as necessary, using Chimera.

Gold Labeling. 2D crystals were applied to gold grids with continuous carbon and allowed to stick for ≈15 sec. Next, the grid was blotted and, sample down, was quickly placed on a droplet that contained fish skin gelatin (diluted 100×; Sigma) for blocking (15–30 min). Then, the grid was washed (4 times, 1–2 min each, using crystallization buffer) before placing on a droplet of either crystallization buffer or antibody solution for 30 min. Four primary antibodies were used in these experiments: an anti HA-epitope antibody (mouse, diluted 1:5,000; Convance), and 3 polyclonal antibodies (rabbit) kindly provided by J. Kaplan (University of Chicago, Chicago) (anti-N terminus (diluted 1:1,000), anti intracellular loop (1:500), and anti-C terminus (1:400). Before use, all antibodies were diluted in crystallization buffer and then spun at high speed to remove large aggregates. After the incubation with the primary antibody, the sample was washed as before (4 drops, 1–2 min each), followed by a 30-min incubation on a droplet that contained 12 nm colloidal gold, conjugated to the appropriate secondary antibody (Jackson ImmunoResearch). After washing, the sample was blotted, and negatively stained with uranyl acetate (1%). All steps were carried out in a plastic container with a lid to prevent drying. A Tecnai 12 TEM equipped with LaB_6 filament was used for the microscopy. Images were acquired on a GATAN 1k1k CCD.

Reconstitution of Apo-CTR1 with Cu(I) and Preparation of Samples for XAS. Apo-hCTR1 was concentrated to ≈10–12 mg/mL in crystallization buffer containing 4 mM DM. Typically, 100 μL of apo-hCTR1 were loaded onto a TCEP column (350 μL of TCEP gel in empty desalting column) allowed to incubate for 15 min, then spun at 8,000 rpm for 2 min. In an inert atmosphere chamber (Coy Lab) a 3-fold or 5-fold excess of tetrakis(acetonitrile)copper(I) hexafluorophosphate [$Cu(MeCN)_4PF_6$] in acetonitrile was added in a volume equivalent to 5 percent of the volume of protein solution to initiate copper loading. The sample was then dialyzed (43) or by passed through 2 consecutive desalting columns (4,000 rpm, 1 min each). An aliquot of each sample was removed for copper and protein analysis. The remainder was mixed with 20% ethylene glycol and frozen in an EXAFS cuvette. Copper was measured by ICPOES on a Perkin–Elmer Optima 2000 instrument. Protein was measured by the Bradford method.

XAS Data Collection and Analysis. Cu K-edge (8.980 keV) extended X-ray absorption fine structure (EXAFS) data for CTR1 and its cysless derivative were collected at the Stanford Synchrotron Radiation Laboratory operating at 3 GeV with currents between 100 and 75 mA. All samples were measured on beam 9–3 using a Si[220] monochromator and a Rh-coated mirror upstream of the monochromator with a 13-keV energy cutoff to reject harmonics. A second Rh mirror downstream of the monochromator was used to focus the beam. Data were collected as fluorescence excitation spectra using a high-count-rate Canberra 30-element Ge array detector with maximum count rates <120 kHz. A nickel oxide filter and Soller slit assembly were placed in front of the detector to reduce the elastic scatter peak. Four to 6 scans of a sample containing only sample buffer were collected at each absorption edge, averaged, and subtracted from the averaged data for the protein samples to remove Ni $K_\beta$fluorescence, and to produce a flat preedge baseline. The samples (80 μL) were measured as aqueous glasses (>20% ethylene glycol) at 10–15 K. Energy calibration was achieved by reference to the first inflection point of a copper metal foil (8,980.3 eV) placed between the second and third ionization chamber. Data reduction and background subtraction were performed with the program modules of EXAFSPAK [George GN (1990) EXAFSPAK, Menlo Park, CA]. Data from each detector channel were inspected for glitches or drop-outs and other nonlinear events before inclusion in the final average. Spectral simulation was carried out with the program EXCURVE 9.2 [Binsted N, Gurman SJ, Campbell JW (1998) EXCURVE 9.2 Warrington, England] (44–46) as described in refs. 43, 47, and 48.

Other Methods. Mutation constructs, fermentation and purification descriptions, disulfide cross-linking experiment description, and more in depth image processing methods are included in the *SI Materials and Methods*.

ACKNOWLEDGMENTS. For the use of their facilities, we thank the Stanford Synchrotron Radiation Laboratory, which is supported by the National Institutes of Health Biomedical Research Technology Program, Division of Re-

search Resources, and by the U.S. Department of Energy, Basic Energy Sciences and Office of Biological and Environmental Research. We thank the Yale School of Medicine for support of the electron cryomicroscopy. This work was supported by National Institutes of Health Grants T32 GM07223 (to C.J.D. and S.G.A.), F31 NS56825 (to C.J.D.), F31 NS045550 (S.G.A.), P01 GM067166 (to N.J.B.), and GM071590 (to V.M.U.)

1. Pena MM, Lee J, Thiele DJ (1999) A delicate balance: Homeostatic control of copper uptake and distribution. *J Nutr* 129:1251–1260.
2. Bremner I (1998) Manifestations of copper excess. *Am J Clin Nutr* 67:1069S–1073S.
3. Winge DR (2002) Copper metalloregulation of gene expression. *Adv Protein Chem* 60:51–92.
4. Maryon EB, Molloy SA, Zimnicka AM, Kaplan JH (2007) Copper entry into human cells: Progress and unanswered questions. *Biometals* 20:355–364.
5. Huffman DL, O'Halloran TV (2001) Function, structure, and mechanism of intracellular copper trafficking proteins. *Annu Rev Biochem* 70:677–701.
6. Kim BE, Nevitt T, Thiele DJ (2008) Mechanisms for copper acquisition, distribution and regulation. *Nat Chem Biol* 4:176–185.
7. Voskoboinik I, Camakaris J (2002) Menkes copper-translocating P-type ATPase (ATP7A): Biochemical and cell biology properties, and role in Menkes disease. *J Bioenerg Biomembr* 34:363–371.
8. Lutsenko S, Efremov RG, Tsivkovskii R, Walker JM (2002) Human copper-transporting ATPase ATP7B (the Wilson's disease protein): Biochemical properties and regulation. *J Bionenerg Biomembr* 34:351–362.
9. Lee J, Pena MM, Nose Y, Thiele DJ (2002) Biochemical characterization of the human copper transporter Ctr1. *J Biol Chem* 277:4380–4387.
10. Bull PC, Thomas GR, Rommens JM, Forbes JR, Cox DW (1993) The Wilson disease gene is a putative copper transporting P-type ATPase similar to the Menkes gene. *Nat Genet* 5:327–337.
11. Vulpe C, Levinson B, Whitney S, Packman S, Gitschier J (1993) Isolation of a candidate gene for Menkes disease and evidence that it encodes a copper-transporting ATPase. *Nat Genet* 3:7–13.
12. de Bie P, Muller P, Wijmenga C, Klomp LW (2007) Molecular pathogenesis of Wilson and Menkes disease: Correlation of mutations with molecular defects and disease phenotypes. *J Med Genet* 44:673–688.
13. Kuo YM, Zhou B, Cosco D, Gitschier J (2001) The copper transporter CTR1 provides an essential function in mammalian embryonic development. *Proc Natl Acad Sci USA* 98:6836–6841.
14. Lee J, Prohaska JR, Thiele DJ (2001) Essential role for mammalian copper transporter Ctr1 in copper homeostasis and embryonic development. *Proc Natl Acad Sci USA* 98:6842–6847.
15. Ishida S, Lee J, Thiele DJ, Herskowitz I (2002) Uptake of the anticancer drug cisplatin mediated by the copper transporter Ctr1 in yeast and mammals. *Proc Natl Acad Sci USA* 99:14298–14302.
16. Komatsu M, et al. (2000) Copper-transporting P-type adenosine triphosphatase (ATP7B) is associated with cisplatin resistance. *Cancer Res* 60:1312–1316.
17. Kuo MT, Chen HH, Song IS, Savaraj N, Ishikawa T (2007) The roles of copper transporters in cisplatin resistance. *Cancer Metastasis Rev* 26:71–83.
18. Banci L, et al. (2006) The Atx1-Ccc2 complex is a metal-mediated protein–protein interaction. *Nat Chem Biol* 2:367–368.
19. Aller SG, Unger VM (2006) Projection structure of the human copper transporter CTR1 at 6-A resolution reveals a compact trimer with a novel channel-like architecture. *Proc Natl Acad Sci USA* 103:3627–3632.
20. Unger VM, Schertler GF (1995) Low resolution structure of bovine rhodopsin determined by electron cryo-microscopy. *Biophys J* 68:1776–1786.
21. Chang G, Spencer RH, Lee AT, Barclay MT, Rees DC (1998) Structure of the MscL homolog from Mycobacterium tuberculosis: A gated mechanosensitive ion channel. *Science* 282:2220–2226.
22. Doyle DA, et al. (1998) The structure of the potassium channel: Molecular basis of K+ conduction and selectivity. *Science* 280:69–77.
23. Bass RB, Strop P, Barclay M, Rees DC (2002) Crystal structure of Escherichia coli MscS, a voltage-modulated and mechanosensitive channel. *Science* 298:1582–1587.
24. Huang Y, Lemieux MJ, Song J, Auer M, Wang DN (2003) Structure and mechanism of the glycerol-3-phosphate transporter from Escherichia coli. *Science* 301:616–620.
25. Abramson J, et al. (2003) Structure and mechanism of the lactose permease of Escherichia coli. *Science* 301:610–615.
26. Eisses JF, Kaplan JH (2005) The mechanism of copper uptake mediated by human CTR1: A mutational analysis. *J Biol Chem* 280:37159–37168.
27. Puig S, Lee J, Lau M, Thiele DJ (2002) Biochemical and genetic analyses of yeast and human high affinity copper transporters suggest a conserved mechanism for copper uptake. *J Biol Chem* 277:26021–26030.
28. Guo Y, Smith K, Lee J, Thiele DJ, Petris MJ (2004) Identification of methionine-rich clusters that regulate copper-stimulated endocytosis of the human Ctr1 copper transporter. *J Biol Chem* 279:17428–17433.
29. Aller SG, Eng ET, De Feo CJ, Unger VM (2004) Eukaryotic CTR copper uptake transporters require two faces of the third transmembrane domain for helix packing, oligomerization, and function. *J Biol Chem* 279:53435–53441.
30. Xiao Z, Loughlin F, George GN, Howlett GJ, Wedd AG (2004) C-terminal domain of the membrane copper transporter Ctr1 from Saccharomyces cerevisiae binds four Cu(I) ions as a cuprous-thiolate polynuclear cluster: Sub-femtomolar Cu(I) affinity of three proteins involved in copper trafficking. *J Am Chem Soc* 126:3081–3090.
31. Xiao Z, Wedd AG (2002) A C-terminal domain of the membrane copper pump Ctr1 exchanges copper(I) with the copper chaperone Atx1. *Chem Commun (Cambridge)* 6:588–589.
32. Wu X, Sinani D, Kim H, Lee J (2008) Copper transport activity of yeast Ctr1 is down regulated via its C-terminus in response to excess copper. *J Biol Chem*: Epub ahead of print.
33. Bagai I, Liu W, Rensing C, Blackburn NJ, McEvoy MM (2007) Substrate-linked conformational change in the periplasmic component of a Cu(I)/Ag(I) efflux system. *J Biol Chem* 282:35695–35702.
34. Loftin IR, Franke S, Blackburn NJ, McEvoy MM (2007) Unusual Cu(I)/Ag(I) coordination of Escherichia coli CusF as revealed by atomic resolution crystallography and X-ray absorption spectroscopy. *Protein Sci* 16:2287–2293.
35. Davis AV, O'Halloran TV (2008) A place for thioether chemistry in cellular copper ion recognition and trafficking. *Nat Chem Biol* 4:148–151.
36. Sinani D, Adle DJ, Kim H, Lee J (2007) Distinct mechanisms for Ctr1-mediated copper and cisplatin transport. *J Biol Chem* 282:26775–26785.
37. Eisses JF, Kaplan JH (2002) Molecular characterization of hCTR1, the human copper uptake protein. *J Biol Chem* 277:29162–29171.
38. Henderson R, et al. (1990) Model for the structure of bacteriorhodopsin based on high-resolution electron cryo-microscopy. *J Mol Biol* 213:899–929.
39. Henderson R, Baldwin JM, Downing K, Lepault J, Zemlin F (1986) Structure of purple membrane from Halobacterium halobium: Recording, measurement and evaluation of electron micrographs at 3.5 Å resolution. *Ultramicroscopy* 19:147–178.
40. Crowther RA, Henderson R, Smith JM (1996) MRC image processing programs. *J Struct Biol* 116:9–16.
41. 4 CCPN (1994) The CCP4 suite: Programs for protein crystallography. *Acta Crystallogr D* 50:760–763.
42. Huang CC, Couch GS, Pettersen EF, Ferrin TE (1996) Chimera: An Extensible Molecular Modeling Application Constructed Using Standard Components. *Pacific Symposium on Biocomputing* 1:724.
43. Ralle M, Lutsenko S, Blackburn NJ (2003) X-ray absorption spectroscopy of the copper chaperone HAH1 reveals a linear two-coordinate Cu(I) center capable of adduct formation with exogenous thiols and phosphines. *J Biol Chem* 278:23163–23170.
44. Binsted N, Hasnain SS (1996) State-of-the-art analysis of whole X-ray absorption spectra. *J Synchrotron Radiat* 3:185–196.
45. Gurman SJ, Binsted N, Ross I (1984) A rapid, exact, curved-wave theory for EXAFS calculations. *J Phys C* 17:143–151.
46. Gurman SJ, Binsted N, Ross I (1986) A rapid, exact, curved-wave theory for EXAFS calculations. II. The multiple-scattering contributions. *J Phys C* 19:1845–1861.
47. Barry AN, Blackburn NJ (2008) A selenocysteine variant of the human copper chaperone for superoxide dismutase. A Se-XAS probe of cluster composition at the domain 3-domain 3 dimer interface. *Biochemistry* 47:4916–4928.
48. Blackburn NJ, Rhames FC, Ralle M, Jaron S (2000) Major changes in copper coordination accompany reduction of peptidylglycine monooxygenase: Implications for electron transfer and the catalytic mechanism. *J Biol Inorg Chem* 5:341–353.